Journal of
Mechanics of Materials and Structures

STABILITY STUDIES FOR CURVED BEAMS

Chong-Seok Chang and Dewey H. Hodges

Volume 4, Nº 7-8 *September 2009*

mathematical sciences publishers

JOURNAL OF MECHANICS OF MATERIALS AND STRUCTURES
Vol. 4, No. 7-8, 2009

STABILITY STUDIES FOR CURVED BEAMS

CHONG-SEOK CHANG AND DEWEY H. HODGES

The paper presents a concise framework investigating the stability of curved beams. The governing equations used are both geometrically exact and fully intrinsic; that is, they have no displacement and rotation variables, with a maximum degree of nonlinearity equal to two. The equations of motion are linearized about either the reference state or an equilibrium state. A central difference spatial discretization scheme is applied, and the resulting linearized ordinary differential equations are cast as an eigenvalue problem. The scheme is validated by comparing predicted numerical results for prebuckling deformation and buckling loads for high arches under uniform pressure with published analytical solutions. This is a conservative system of forces despite their being modeled as distributed follower forces. The results show that the stretch-bending coupling term must be included in order to accurately calculate the prebuckling curvature and bending moment of high arches. In addition, the lateral-torsional buckling instability of curved beams under tip moments is investigated. Finally, when a curved beam is loaded with nonconservative forces, resulting dynamic instabilities may be found through the current framework.

1. Introduction

For decades, the vibration of curved beams, rings, and arches has been extensively investigated. About 400 references, which cover the in-plane (i.e., in the plane of the undeformed, initially curved beam), out-of-plane (i.e., out of the plane of the undeformed, initially curved beam), coupled, linear and nonlinear vibrations, have been summarized by in [Chidamparam and Leissa 1993]. While linear theory is adequate for free-vibration analysis of initially curved beams, one must linearize the equations of nonlinear theory about a static equilibrium state, if a beam is brought into a state of high curvature by the loads acting on it. Because of this, the behavior of a beam curved under load may differ substantially from that of an initially curved beam of identical geometry. The geometrically exact and fully intrinsic theory of curved and twisted beams in [Hodges 2003] provides an excellent framework in which to elegantly study the coupled vibration characteristics of curved beams, particularly those curved because they are loaded. This is because of the simplicity of the equations — so simple that each term of every equation can be easily interpreted intuitively. There are no displacement or rotation variables (this is what is meant by "intrinsic" in this context); as a result there are no nonlinearities of degree greater than two. Both finite element and finite difference discretization schemes are easily applied to these equations for numerical computation, and the framework presented herein is simpler than that of other nonlinear beam theories. Because of these observations, we have revisited the topic and broadened the base of cases studied.

This paper provides details of how to make use of the fully intrinsic formulation for calculating vibration frequencies and buckling loads of curved beams. One aspect of these calculations that is substantially different from the usual approach involves the way boundary conditions are enforced. In [Chang and

Keywords: elastic stability, structural stability, buckling, elastica, fully intrinsic.

Hodges 2009] results from free-vibration analysis of curved beams were compared with those from published work. Chidamparam and Leissa [1995], Tarnopolskaya et al. [1996], and Fung [2004] focused on in-plane vibration; and Irie et al. [1982] and Howson and Jemah [1999] on out-of-plane vibration. The coupled free-vibration frequencies were also presented as part of an investigation of low-frequency mode transition, also referred to as veering [Tarnopolskaya et al. 1999; Chen and Ginsberg 1992].

It was shown analytically by Hodges [1999] and Simitses and Hodges [2006] that initially curved isotropic beams possess stretch-bending elastic coupling, that this coupling is proportional to initial curvature when the beam reference line is along the locus of cross-sectional centroids, and that this coupling cannot be ignored when calculating the equilibrium state of high circular arches. Although this term does not affect the buckling load, it must be included to calculate the prebuckling state correctly. As a validation exercise, the present formulation is applied to the prebuckling deformation of high arches. Displacement, curvature, bending moment and bifurcation load are compared to the analytical solutions with and without this coupling term.

As a more powerful alternative than analytical treatments for determining cross-sectional elastic constants, one may use VABS (variational asymptotic beam sectional analysis) [Cesnik and Hodges 1997; Yu et al. 2002; Hodges 2006] to numerically calculate all the cross-sectional elastic constants, including the stretch-bending coupling term. Based on results obtained from VABS, it is easy to show that there is another term that depends on initial curvature and reflects shear-twist coupling. This term becomes zero if the beam reference axis is along the locus of sectional shear centers. The location of the sectional shear center depends on the initial curvature, but an analytical expression for that dependence is unknown. Therefore, without a cross-sectional analysis tool such as VABS, which provides accurate cross-sectional elastic constants as a function of initial curvature, certain aspects of the analysis presented herein would be impossible.

2. Intrinsic beam formulation

The geometrically exact, intrinsic governing equations of [Hodges 2003] for the dynamics of an initially curved and twisted, generally anisotropic beam are

$$\begin{aligned} F_B' + \widetilde{K_B} F_B + f_B &= \dot{P}_B + \widetilde{\Omega_B} P_B, \\ M_B' + \widetilde{K_B} M_B + (\widetilde{e_1} + \widetilde{\gamma}) F_B + m_B &= \dot{H}_B + \widetilde{\Omega_B} H_B + \widetilde{V_B} P_B, \\ V_B' + \widetilde{K_B} V_B + (\widetilde{e_1} + \widetilde{\gamma}) \Omega_B &= \dot{\gamma}, \\ \Omega_B' + \widetilde{K_B} \Omega_B &= \dot{\kappa}, \end{aligned} \tag{1}$$

where F_B and M_B are the internal force and moment measures, P_B and H_B are the sectional linear and angular momenta, V_B and Ω_B are the velocity and angular velocity measures, γ and κ are the force and moment strain measures, k contains the initial twist and curvature measures of the beam, $K_B = k + \kappa$ contains the total curvature measures, and f_B and m_B are external force and moment measures, where loads such as gravitational, aerodynamic, and mechanical applied loads are taken into account. All quantities are expressed in the basis of the deformed beam cross-sectional frame except k which is in the basis of the undeformed beam cross-sectional frame. The tilde operator as in $\widetilde{a}b$ reflects a matrix form

of the cross product of vectors $\mathbf{a} \times \mathbf{b}$ when both vectors and their cross product are all expressed in a common basis.

A central difference discretization scheme is applied to the intrinsic governing equations in space to obtain a numerical solution. The scheme satisfies both of the space-time conservation laws derived in [Hodges 2003]. This scheme can be viewed as equivalent to a particular finite element discretization, and the intrinsic governing equations are expressed as element and nodal equations. The n-th element equations, which are a spatially discretized form of (1), are

$$\begin{aligned}
\frac{\widehat{F}_l^{n+1} - \widehat{F}_r^n}{dl} + (\widetilde{\overline{\kappa}}^n + \widetilde{k}^n)\overline{F}^n + \overline{f}^n - \dot{\overline{P}}^n - \widetilde{\overline{\Omega}}^n \overline{P}^n = 0,\\
\frac{\widehat{M}_l^{n+1} - \widehat{M}_r^n}{dl} + (\widetilde{\overline{\kappa}}^n + \widetilde{k}^n)\overline{M}^n + (\widetilde{e_1} + \widetilde{\overline{\gamma}}^n)\overline{F}^n + \overline{m}^n - \dot{\overline{H}}^n - \widetilde{\overline{\Omega}}^n \overline{H}^n - \widetilde{\overline{V}}^n \overline{P}^n = 0,\\
\frac{\widehat{V}_l^{n+1} - \widehat{V}_r^n}{dl} + (\widetilde{\overline{\kappa}}^n + \widetilde{k}^n)\overline{V}^n + (\widetilde{e_1} + \widetilde{\overline{\gamma}}^n)\overline{\Omega}^n - \dot{\overline{\gamma}}^n = 0,\\
\frac{\widehat{\Omega}_l^{n+1} - \widehat{\Omega}_r^n}{dl} + (\widetilde{\overline{\kappa}}^n + \widetilde{k}^n)\overline{\Omega}^n - \dot{\overline{\kappa}}^n = 0,
\end{aligned} \tag{2}$$

where $\overline{f}^n$ and $\overline{m}^n$ include any external forces and moments applied to the n-th element and dl is the length of an element.

The equations for node n need to include possible discontinuities caused by a nodal mass, a nodal force, and a slope discontinuity, so that

$$\begin{aligned}
\widehat{F}_r^n - \widehat{C}_{lr}^{n^T} \widehat{F}_l^n + \widehat{f}^n - \dot{\widehat{P}}_r^n - \widetilde{\widehat{\Omega}}_r^n \widehat{P}_r^n = 0,\\
\widehat{M}_r^n - \widehat{C}_{lr}^{n^T} \widehat{M}_l^n + \widehat{m}^n - \dot{\widehat{H}}_r^n - \widetilde{\widehat{\Omega}}_r^n \widehat{H}_r^n - \widetilde{\widehat{V}}_r^n \widehat{P}_r^n = 0,
\end{aligned} \tag{3}$$

where $\widehat{C}_{lr}$ reflects the slope discontinuity, $\widehat{f}^n$ and $\widehat{m}^n$ are external forces and moments applied at n-th node, and

$$\widehat{V}_l^n = \widehat{C}_{lr}^n \widehat{V}_r^n \quad \text{and} \quad \widehat{\Omega}_l^n = \widehat{C}_{lr}^n \widehat{\Omega}_r^n. \tag{4}$$

One may also include gravitational force in the analysis. When this is done, the formulation needs additional equations to keep track of the vertical direction expressed in the cross-sectional basis vectors of the deformed beam; details may be found in [Patil and Hodges 2006]. This aspect of the analysis is not needed for the problems addressed herein.

3. Boundary conditions

Boundary conditions are needed to complete the formulation. Here, we describe boundary conditions for pinned–pinned and clamped–clamped beams. At each end, for the static case, either natural boundary conditions in terms of $\widehat{F}$ and $\widehat{M}$ or geometric boundary conditions in terms of u and C^{iB} may be prescribed. Here u is a column matrix of displacement measures u_i in the cross-sectional frame of the undeformed beam. Although these geometric boundary conditions are in terms of displacement and rotation variables, they are easily expressed in terms of other variables such as κ, γ, etc., given in (12), keeping the formulation intrinsic.

If displacement and rotation variables appear in the boundary conditions for the free-vibration case, a numerical Jacobian becomes necessary since an analytical determination of it would become intractable. Fortunately, when calculating free-vibration frequencies, one may for convenience replace boundary conditions on displacement and rotation variables with boundary conditions in terms of generalized velocities $\widehat{V}$ and $\widehat{\Omega}$. With the velocity boundary conditions, rigid-body modes will not be eliminated from results.

3.1. ***Pinned–pinned boundary conditions.*** A total of 12 boundary conditions is necessary to calculate free-vibration frequencies, given by

$$\widehat{V}_r^1 = \widehat{M}_l^1 = 0, \tag{5}$$

$$\widehat{V}_r^{N+1} = 0 \quad \text{or} \quad \begin{cases} e_1^T C^{iB^{N+1}} \widehat{F}_r^{N+1} = 0, \\ e_2^T \widehat{V}_r^{N+1} = 0, \\ e_3^T C^{iB^{N+1}} \widehat{V}_r^{N+1} = 0, \end{cases} \tag{6}$$

$$\widehat{M}_r^{N+1} = 0, \tag{7}$$

where $C^{iB^{N+1}}$ is the rotation matrix of the beam cross-section at the right end. Equation (5) fixes the left boundary in space but leaves it free to rotate about all three axes. One may either apply a geometric boundary condition of zero displacement at left end or may take advantage of the intrinsic formulation through applying the velocity boundary condition given in (5). The right boundary condition of (6) allows free movement in the axial direction while holding velocity components in the transverse directions to zero, as shown in the right part of Figure 1. When there are no applied loads, one may simply make use of trivial values as reference states.

For a loaded case, however, the reference states should be obtained from a specific static equilibrium. To determine the static equilibrium, six boundary conditions are necessary, given by

$$\widehat{M}_l^1 = 0, \tag{8}$$

$$u_1^{N+1} = 0 \quad \text{or} \quad e_1^T C^{iB^{N+1}} \widehat{F}_r^{N+1} = 0, \qquad u_2^{N+1} = u_3^{N+1} = 0. \tag{9}$$

The right end can be chosen either to be fixed in space or free to move in the axial direction, which is described in (9). For static equilibrium, one must apply displacement boundary conditions, which appear in (9), instead of velocity boundary conditions.

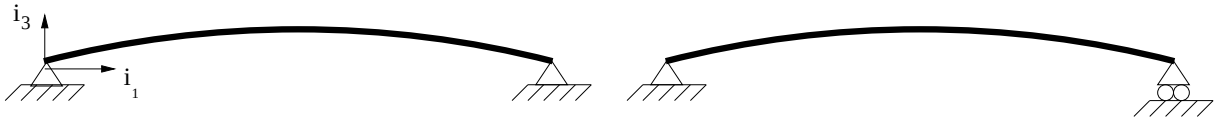

Figure 1. Schematics of initially curved beams with pinned–pinned boundary conditions.

Figure 2. Initially curved beam with clamped–clamped boundary condition.

3.2. ***Clamped–clamped boundary conditions.*** The clamped-clamped boundary conditions are

$$\widehat{V}_r^1 = \widehat{\Omega}_r^1 = 0 \quad \text{and} \quad \widehat{V}_r^{N+1} = \widehat{\Omega}_r^{N+1} = 0, \tag{10}$$

describing boundaries fixed in space and with zero rotation about all three axes.

As in the case of the pinned–pinned boundary condition, the boundary conditions for static equilibrium of a loaded case must be written in terms of displacement and rotation, given by

$$u_{\text{def}}^{N+1} = 0 \quad \text{and} \quad \widehat{C}_{\text{undef}}^{iB^{N+1}{}^T} \widehat{C}_{\text{def}}^{iB^{N+1}} = \Delta, \tag{11}$$

where u_{def} is the column matrix of displacement measures at the right end of the beam, $\widehat{C}_{\text{def}}^{iB^{N+1}}$ is the rotation matrix of the beam cross-section at the right end after deformation, and $\widehat{C}_{\text{undef}}^{iB^{N+1}}$ is the rotation matrix of the beam cross-section at the right end in the undeformed state.

The boundary conditions associated with geometric conditions for static equilibrium require displacement and/or rotation to be expressed. These are described by the generalized strain-displacement equations from [Hodges 2003], given by

$$(r+u)' = C^{iB}(\gamma + e_1) \quad \text{and} \quad C^{Bi\,\prime} = -(\widetilde{\kappa} + \widetilde{k}) C^{Bi}, \tag{12}$$

where r is the column matrix of position vector measures and u is the column matrix of displacement measures, both in the undeformed beam cross-sectional basis, and C^{Bi} is the rotation matrix of the beam cross-sectional reference frame in the deformed configuration. Equation (12) can be discretized as

$$\begin{aligned} r^{n+1} + u^{n+1} &= r^n + u^n + \overline{C}^{iB^n}(\overline{\gamma}^n + e_1) dl, \\ \widehat{C}^{Bi^{n+1}} &= \left(\frac{\Delta}{dl} + \frac{\widetilde{\overline{\kappa}} + \widetilde{\overline{k}}^n}{2}\right)^{-1} \left(\frac{\Delta}{dl} - \frac{\widetilde{\overline{\kappa}} + \widetilde{\overline{k}}^n}{2}\right) \widehat{C}^{Bi^n}. \end{aligned} \tag{13}$$

4. Linearization

The governing equations in the previous section are linearized about a static equilibrium so that they reduce to an eigenvalue problem to calculate the free-vibration frequencies. First,

$$X = X_{eq} + X^*(t), \tag{14}$$

where X is a state, X_{eq} is a value of the state at a static equilibrium, and X^* is small perturbation about the static value of the state. The linearized element equations from the intrinsic beam formulation are then

$$\begin{aligned} \frac{\widehat{F}_l^{*n+1} - \widehat{F}_r^{*n}}{dl} + (\widetilde{\overline{\kappa}_{eq}^n} + \widetilde{k}^n)\overline{F}^{*n} + \widetilde{\overline{\kappa}^{*n}}\,\overline{F}_{eq}^n + \mu^n \overline{g}^{*n} &= \dot{\overline{P}}^{*n}, \\ \frac{\widehat{M}_l^{*n+1} - \widehat{M}_r^{*n}}{dl} + (\widetilde{\overline{\kappa}_{eq}^n} + \widetilde{k}^n)\overline{M}^{*n} + \widetilde{\overline{\kappa}^{*n}}\,\overline{M}_{eq}^n + (\widetilde{e}_1 + \widetilde{\overline{\gamma}_{eq}^n})\overline{F}^{*n} + \widetilde{\overline{\gamma}^{*n}}\,\overline{F}_{eq}^n + \mu^n \widetilde{\xi}^n \overline{g}^{*n} &= \dot{\overline{H}}^{*n}, \\ \frac{\widehat{V}_l^{*n+1} - \widehat{V}_r^{*n}}{dl} + (\widetilde{\overline{\kappa}_{eq}^n} + \widetilde{k}^n)\overline{V}^{*n} + (\widetilde{e}_1 + \widetilde{\overline{\gamma}_{eq}^n})\overline{\Omega}^{*n} &= \dot{\overline{\gamma}}^{*n}, \\ \frac{\widehat{\Omega}_l^{*n+1} - \widehat{\Omega}_r^{*n}}{dl} + (\widetilde{\overline{\kappa}_{eq}^n} + \widetilde{k}^n)\overline{\Omega}^{*n} &= \dot{\overline{\kappa}}^{*n}. \end{aligned} \tag{15}$$

The linearized nodal equations are

$$\widehat{F}_r^{*n} - \widehat{C}_{lr}^{n^T}\widehat{F}_l^{*n} + \widehat{\mu}^n\widehat{g}_r^{*n} - \dot{\widehat{P}}_r^{*n} = 0 \quad \text{and} \quad \widehat{M}_r^{*n} - \widehat{C}_{lr}^{n^T}\widehat{M}_l^{*n} + \widehat{\mu}^n\widetilde{\widehat{\xi}}^n\widehat{g}_r^{*n} - \dot{\widehat{H}}_r^{*n} = 0. \tag{16}$$

These linearized equations of motion can be expressed in a matrix form as $A\dot{X}^* = BX^*$, which is a system of first-order ordinary differential equations. When $X^* = \check{X}\exp(\lambda t)$ is assumed, the system is easily cast as a generalized eigenvalue problem of the form $B\check{X} = A\lambda\check{X}$. When B^{-1} exists, the equations reduce to a standard eigenvalue problem, such that $\lambda^{-1}\check{X} = B^{-1}A\check{X}$. When the eigenvalues are pure imaginary, the motion is simple harmonic.

5. Validation

A typical cross-sectional model for a beam has the form

$$\begin{Bmatrix} \gamma_{11} \\ 2\gamma_{12} \\ 2\gamma_{13} \\ \kappa_1 \\ \kappa_2 \\ \kappa_3 \end{Bmatrix} = \begin{bmatrix} R_{11} & R_{12} & R_{13} & S_{11} & S_{12} & S_{13} \\ R_{12} & R_{22} & R_{23} & S_{21} & S_{22} & S_{23} \\ R_{13} & R_{23} & R_{33} & S_{31} & S_{32} & S_{33} \\ S_{11} & S_{21} & S_{31} & T_{11} & T_{12} & T_{13} \\ S_{12} & S_{22} & S_{32} & T_{12} & T_{22} & T_{23} \\ S_{13} & S_{23} & S_{33} & T_{13} & T_{23} & T_{33} \end{bmatrix} \begin{Bmatrix} F_1 \\ F_2 \\ F_3 \\ M_1 \\ M_2 \\ M_3 \end{Bmatrix} \tag{17}$$

or

$$\begin{Bmatrix} \gamma \\ \kappa \end{Bmatrix} = \begin{bmatrix} R_{3\times3} & S_{3\times3} \\ S_{3\times3}^T & T_{3\times3} \end{bmatrix} \begin{Bmatrix} F \\ M \end{Bmatrix}, \tag{18}$$

where the 3×3 submatrices R, S, and T, which make up the cross-sectional flexibility matrix, may be computed by VABS for various initial curvatures [Cesnik and Hodges 1997; Yu et al. 2002; Hodges 2006]. When the reference line of the beam is chosen to be coincident with a cross-section shear center, the shear-torsion elastic couplings S_{21} and S_{31} vanish for that section.

Results in this section are to be compared with the analytical solutions for high arches in [Hodges 1999] and [Simitses and Hodges 2006]. Hydrostatic pressure is modeled as a distributed follower force with constant magnitude per unit deformed length. When the equations are applied to buckling, the boundaries are allowed (artificially) to move so as to maintain a circular arc in the deformed but prebuckled state. For this case, only the radial displacement u_2 and local stretching strain measure ε are nontrivial and they are given as

$$\overline{u}_2 = \frac{\lambda\rho^2}{1+\lambda\rho^2} \quad \text{and} \quad \overline{\varepsilon} = -\overline{u}_2, \tag{19}$$

where $\rho^2 = I_3/AR^2$ and $\lambda = f_2R^3/EI_3$, where $EI_3 = 1/T_{33}$. (Subscript 2 indicates the radial direction along $\mathbf{b}_2$ and subscript 3 indicates normal to the plane of the undeformed arch. For more details on the definition of parameters see [Hodges 1999] and [Simitses and Hodges 2006].) Figure 3 shows the excellent agreement between published analytical and present numerical solutions for ε versus λ.

Next, numerical results from the present analysis are compared with published analytical solutions for pinned–pinned and clamped–clamped arches under hydrostatic pressure. When the boundary conditions are not artificially adjusted, the problem is far more interesting. The geometry of the curved beam or arch

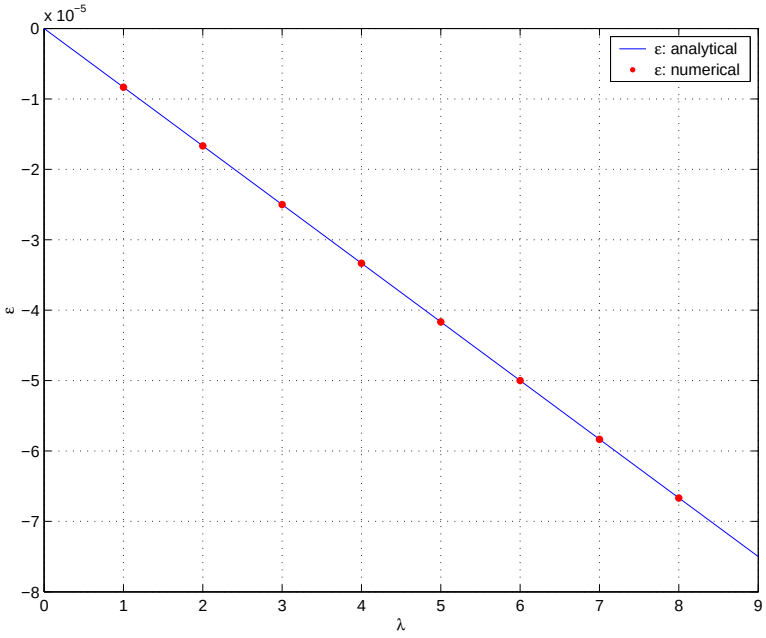

Figure 3. Plot of ε versus λ for $\rho^2 = 8.3333 \times 10^{-6}$, $\alpha = 1$.

used for the results is such that $\ell = 20$ m and $hk_2 = h/R_r = 0.01$, where h is the height of the cross-section, $R_r = 1/k_2$ is the initial radius of curvature, k_2 is the initial curvature, and α is the half-angle ($\ell = 2R_r\alpha$).

The prebuckling tangential and radial displacements u_1 and u_2, prebuckling curvature κ and bending moment M for the pinned–pinned case are shown in Figures 4 and 5. All quantities are normalized according to the scheme in [Hodges 1999]. The present results agree well with the analytical solutions

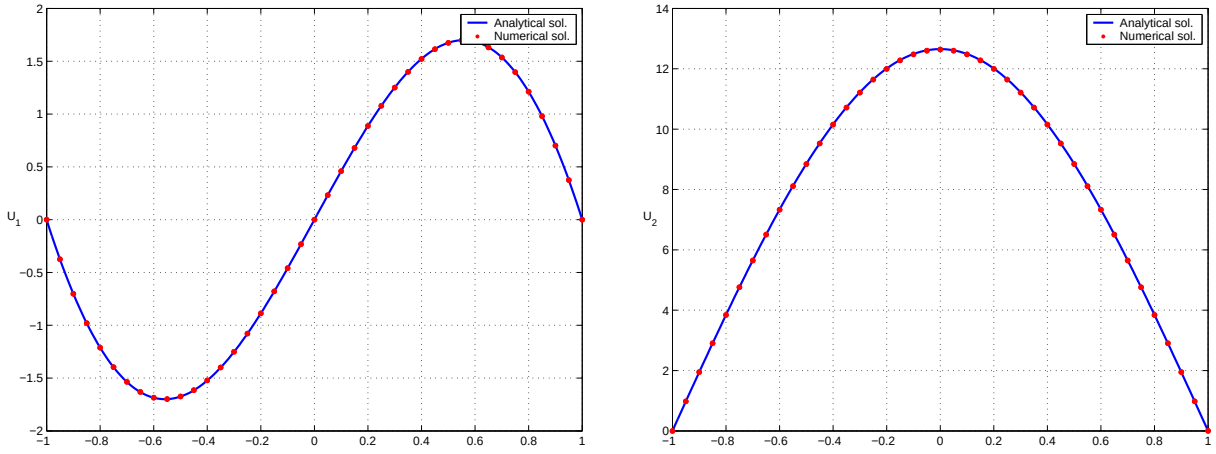

Figure 4. Normalized displacements u_1, u_2 for the pinned-pinned case ($\rho^2 = 8.3333 \times 10^{-6}$, $\lambda = 8$, $\alpha = 1$).

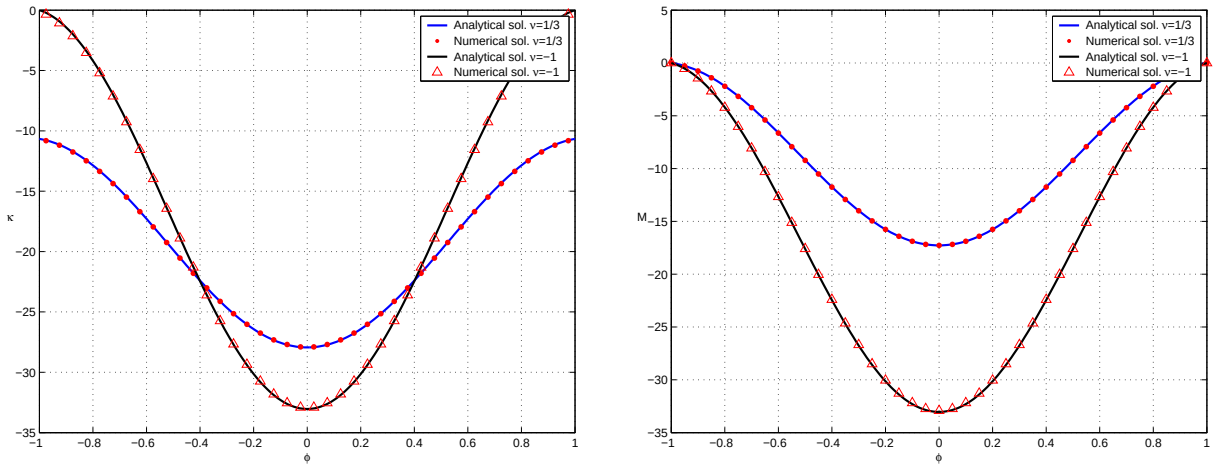

Figure 5. Curvature κ and bending moment M for the pinned-pinned case ($\rho^2 = 8.3333 \times 10^{-6}$, $\lambda = 8$, $\alpha = 1$).

for both $\nu = 1/3$ and $\nu = -1$; note that $\nu = -1$ annihilates the stretch-bending coupling according to both the analytical solution and the cross-sectional flexibility coefficients obtained from VABS. As is the case with the analytical solutions, κ and M depend significantly on whether or not the coupling term is included. Incidentally, there is a typographical error in the captions of Figures 2 and 3 in [Hodges 1999]; the results presented are for $\lambda = 8$, not $\lambda = 5$.

The results for the same beam and same loading but with clamped–clamped boundary conditions are shown in Figure 6 and 7. Only the normalized prebuckling bending moments change with ν, as is the case with the analytical solution in [Hodges 1999].

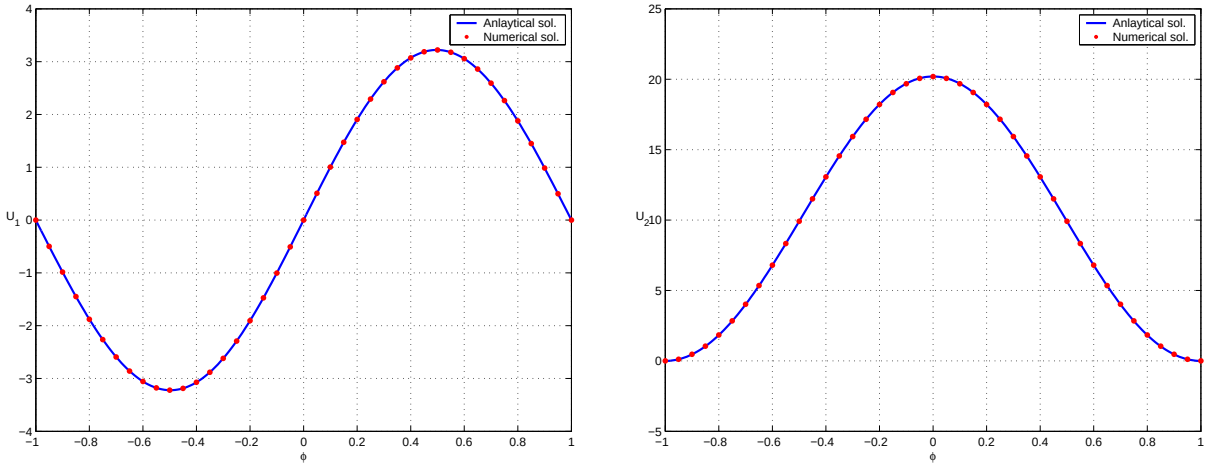

Figure 6. Normalized displacements u_1, u_2 for the clamped-clamped case ($\rho^2 = 8.3333 \times 10^{-6}$, $\lambda = 8$, $\alpha = 1$).

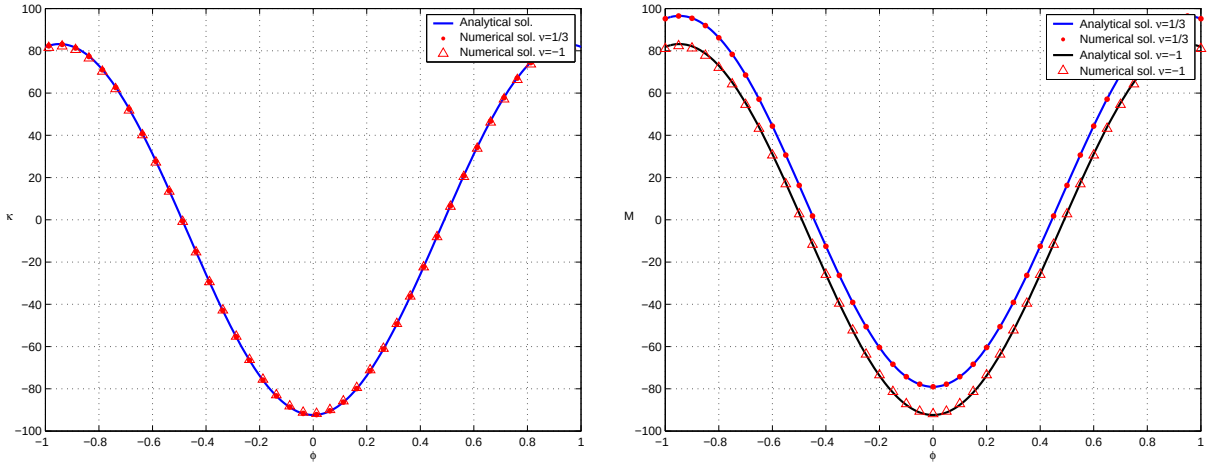

Figure 7. Curvature κ and bending moment M for the clamped-clamped case ($\rho^2 = 8.3333 \times 10^{-6}$, $\lambda = 8$, $\alpha = 1$).

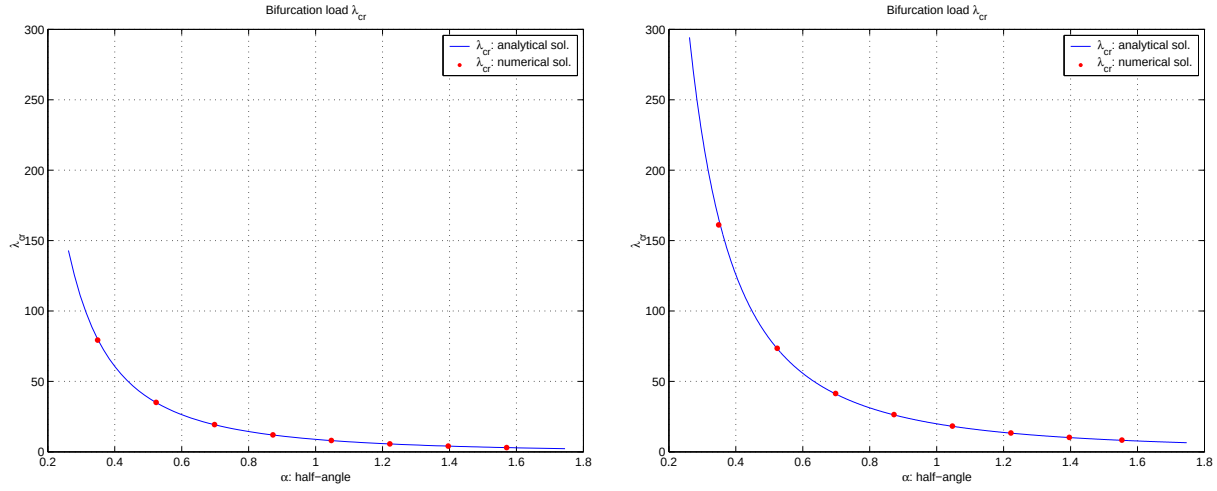

Figure 8. λ_{cr} versus α for $\rho^2 = 8.3333 \times 10^{-6}$ (left for pinned–pinned and right for clamped–clamped cases).

As the distributed follower force increases, the high arch will be buckled. For the pinned–pinned case, the bifurcation load is $\lambda_{\text{cr}} = \pi^2/\alpha^2 - 1$ and for the clamped–clamped case, the characteristic equation for the bifurcation load is

$$k \tan \alpha \cot k\alpha = 1,$$

where $k = \sqrt{1+\lambda}$, as given in [Simitses and Hodges 2006]. For various half-angles, the bifurcation loads are computed and shown in Figure 8. Thus, the present approach is seen to provide an excellent numerical framework to study prebuckled deformation and buckling analysis without ad hoc modeling approximations.

6. Lateral-torsional buckling instability of curved beams under end moments

In this study the stability characteristics of curved beams are considered, including beams both with curvature that is built-in and curvature that occurs because the beam is loaded with end moments. The end moments are applied keeping its original orientation to the beam cross-section in deformation configuration, which are nonconservative. The section properties vary according to the initial curvature. Sample results are given in Table 1. In the general case we consider an curved beam with various initial curvatures k_2 loaded under various equal and opposite values of applied moments at the ends giving rise to a constant value of bending moment $\overline{M}_2$. To facilitate this parametric study, the total static equilibrium value of curvature $\overline{K}_2$ is divided into two parts: the initial curvature k_2 and the curvature caused by the applied end moments $\overline{M}_2/EI_2$. The total curvature can then be expressed as

$$\overline{K}_2 = k_2 + \frac{\overline{M}_2}{EI_2}, \tag{20}$$

where EI_2 is the in-plane bending stiffness for bending in the plane of the curved beam. A nondimensional curvature ratio β is then introduced, where β is the ratio of the initial curvature to the final total curvature and defined as

$$\beta = \frac{k_2}{\overline{K}_2} \qquad (\overline{K}_2 \neq 0). \tag{21}$$

If $\beta = 0$, the beam has a zero initial curvature. If $\beta = 1$, the beam's initial curvature is the total curvature, which means that no end moments will be applied. If $\beta = -1$, the beam has an opposite initial curvature to the final configuration. The first three parts of Figure 9 show the cases $\beta = -1, 0, 1$. End moments are applied to deform the beam so that $\overline{K}_2 = -0.1$, as shown in the last part of the same figure. A rectangular cross-section is chosen to determine beam properties.

Table 2 and Figure 10 show the vibration frequencies for various β. It shows that the frequencies of modes 2 and 6 change as β changes. The frequency of mode 2, in which the first out-of-plane bending motion dominates, decreases as β decreases, becoming zero when $\beta = -0.0117$. This critical β is named

R_r	1/0.1	1/0.07	1/0.04	1/0.01
R_{11}	$1.4286 \cdot 10^{-9}$	$1.4286 \cdot 10^{-9}$	$1.4286 \cdot 10^{-9}$	$1.4286 \cdot 10^{-9}$
R_{22}	$4.7292 \cdot 10^{-9}$	$4.7291 \cdot 10^{-9}$	$4.7291 \cdot 10^{-9}$	$4.7291 \cdot 10^{-9}$
R_{33}	$4.7291 \cdot 10^{-9}$	$4.7291 \cdot 10^{-9}$	$4.7291 \cdot 10^{-9}$	$4.7291 \cdot 10^{-9}$
S_{12}	$3.4133 \cdot 10^{-10}$	$2.3790 \cdot 10^{-10}$	$1.3619 \cdot 10^{-10}$	$3.4476 \cdot 10^{-11}$
S_{21}	$-1.1431 \cdot 10^{-12}$	$8.6327 \cdot 10^{-13}$	$9.5232 \cdot 10^{-14}$	$-6.7113 \cdot 10^{-13}$
T_{11}	$2.7802 \cdot 10^{-6}$	$2.7803 \cdot 10^{-6}$	$2.7803 \cdot 10^{-6}$	$2.7803 \cdot 10^{-6}$
T_{22}	$1.7143 \cdot 10^{-6}$	$1.7143 \cdot 10^{-6}$	$1.7143 \cdot 10^{-6}$	$1.7143 \cdot 10^{-6}$
T_{33}	$1.7143 \cdot 10^{-6}$	$1.7143 \cdot 10^{-6}$	$1.7143 \cdot 10^{-6}$	$1.7143 \cdot 10^{-6}$
ξ_3	$8.7588 \cdot 10^{-5}$	$6.1310 \cdot 10^{-5}$	$3.5034 \cdot 10^{-5}$	$8.7585 \cdot 10^{-6}$

Table 1. Nonzero cross-sectional constants used for calculation of coupled free-vibration frequencies for initially curved beams: flexibility submatrices R_{ij}, S_{ij}, T_{ij}, radius of curvature R_r, and shear center location ξ_3.

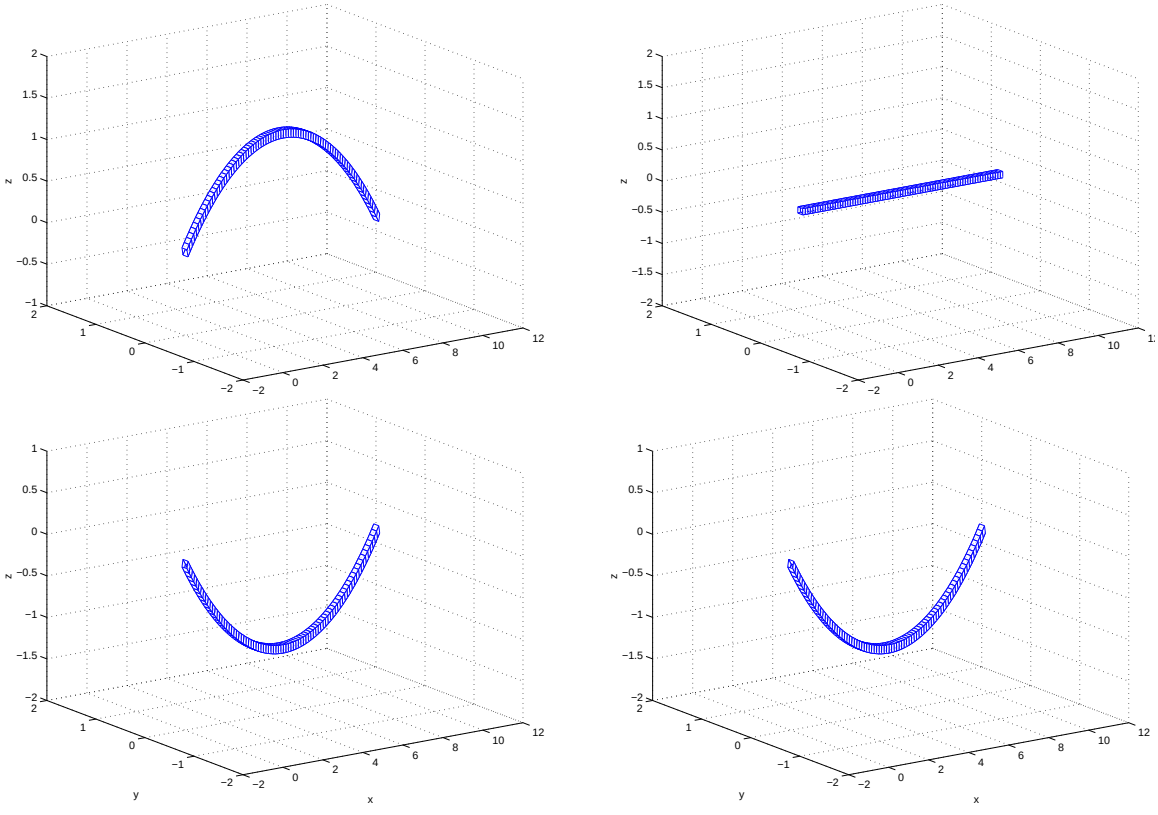

Figure 9. Initial configurations of beams with $\beta = -1$ (top left), $\beta = 0$ (top right), and $\beta = 1$ (bottom left). Bottom right: Final deformed configuration ($\overline{K}_2 = -0.1$) with end moments.

β_{cr}, indicating that this case is at the stability boundary and the lateral-torsional buckling instability will occur if $\beta < \beta_{\text{cr}} = -0.0117$.

The lateral-torsional buckling instability depends on the in- and out-of-plane bending stiffnesses and the torsional stiffness, which convey how deep the beam is. For this example with a rectangular cross-section, each stiffness will be determined by the ratio of cross-section $r = h/b$. So various cases for different r and same cross-sectional area $\Omega_{\text{area}} = bh/\ell^2$ are studied to determine β_{cr}. β_{cr} indicates that for the

β	mode 1	mode 2	mode 3	mode 4	mode 5	mode 6
0	31.842	32.548	89.567	90.630	177.94	179.13
0.1	31.842	96.606	89.567	90.209	177.94	185.45
0.2	31.842	125.16	89.567	89.776	177.94	199.11
0.3	31.842	140.08	89.332	89.568	177.94	211.83
0.4	31.842	147.61	88.878	89.568	177.94	229.92
0.5	31.842	151.58	88.412	89.568	177.95	248.30

Table 2. Vibration frequencies (ω_{freq}) versus curvature ratio (β).

given cross-section, the instability will occur if the initial curvature k_2 is larger than $-0.1\beta_{\mathrm{cr}}$ when the total static equilibrium curvature $\overline{K}_2 = -0.1$. Figure 11 shows the critical values β_{cr} for $\Omega_{\mathrm{area}} = 0.01, \sim 0.1$, and ~ 0.2. The region above the lines are free of the lateral-torsional buckling instability and the buckling will occur if a case is under the line. As the cross-sectional area gets small and the ratio r increases, that is, the beam gets deeper, the example is prone to the lateral-torsional instability as shown in Figure 11.

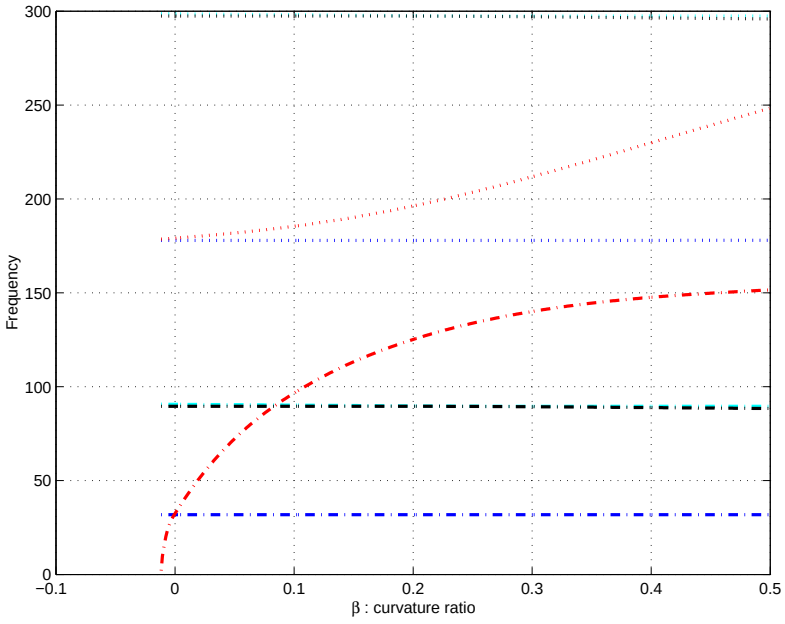

Figure 10. Vibration frequencies (ω_{freq}) versus curvature ratio (β).

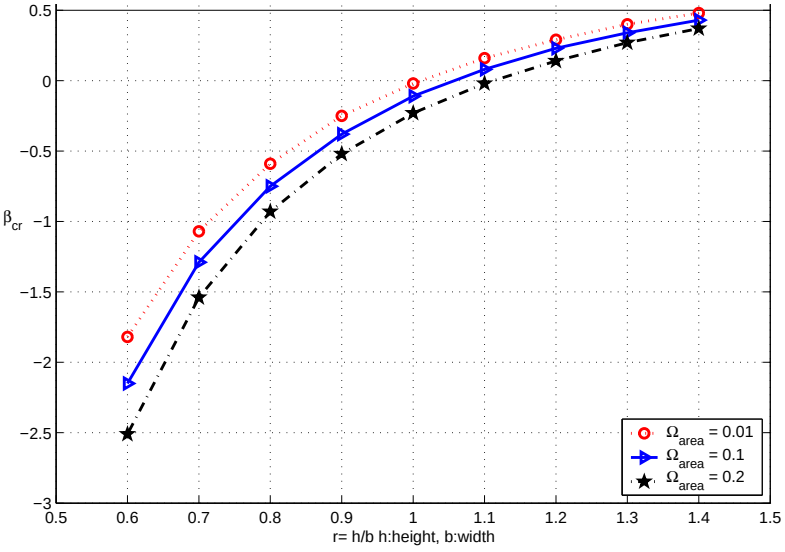

Figure 11. Critical curvature ratio β_{cr} versus $r = h/b$ for the lateral-torsional buckling instability.

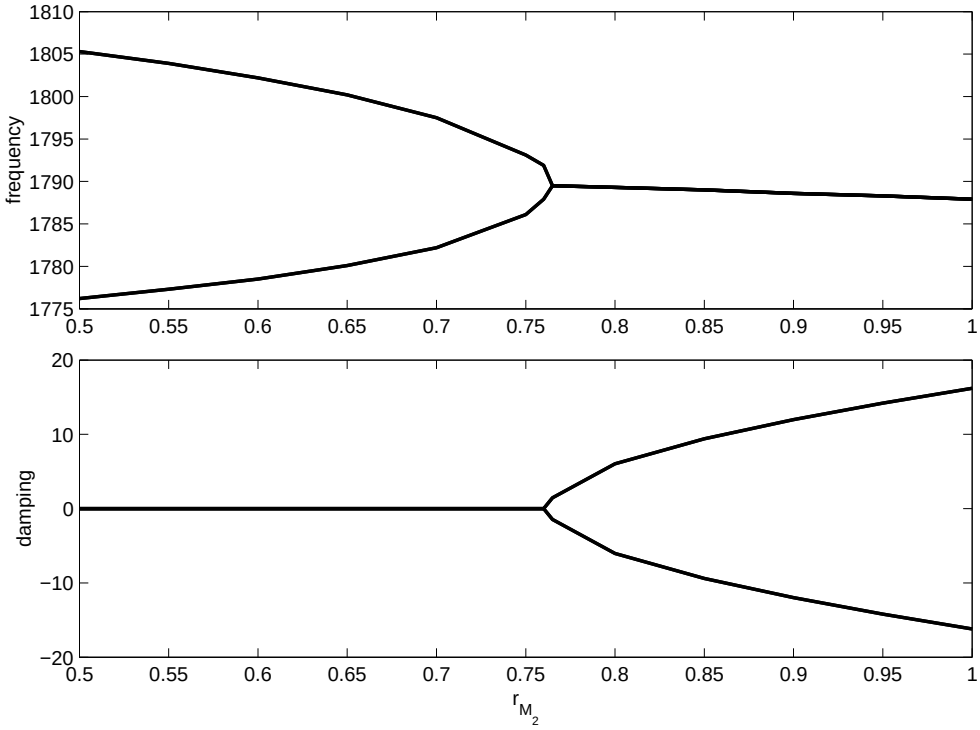

Figure 12. Frequencies and damping for different end moments ($\beta = -0.02$, $r = 1.1$, $\Omega_{\text{area}} = 0.2$).

For deep beams loaded with nonconservative end moments, one may also encounter a lateral-torsional flutter instability. The dynamic instability might occur before the lateral-torsional instability occurs. A further study is done for the case with $\beta = -0.02$, $r = 1.1$, $\Omega_{\text{area}} = 0.2$, which is one case of the lateral-torsional buckling instability boundary curves shown in Figure 11. For this case, the applied tip moment is $\overline{M}_2 = -EI_2(0.1 + k_2) = -0.1002EI_2$, which we denote as the reference value $M_{2,\text{ref}}$. Another instability can be found through lowering the ratio $r_{M_2} = M_2/M_{2,\text{ref}}$. Then, the second torsional and third out-of-plane bending modes shown in Figure 12 become oscillatory with increasing amplitude if $r_{M_2} \geq 0.765$. For this case, the dynamic instability occurs prior to the lateral-torsional instability.

7. Conclusion

The paper describes a numerical procedure of intrinsic beam formulation to study the stability of curved beams under certain types of loading. The linear analysis provides the vibration frequencies about the equilibrium state for given arbitrary configurations undergoing given loads. Present results of prebuckled in-plane deformation and buckling analysis agree well with those from the published paper of high arches. Additional parametric study determines the stability boundaries for the system. For nonconservatively loaded systems, as the example shows, the dynamic instability also can be identified.

The governing equations of the present approach do not require displacement and rotation variables. Even though the displacement and rotation variables appear in the boundary conditions, those variables

are easily recovered from the formulation (i.e. they are secondary variables and can be expressed in terms of the primary variables). This makes the whole analysis quite concise, reducing computational time. Thus, the present approach is an excellent numerical framework to study prebuckled deformation and buckling analysis for curved beams with better understanding.

References

[Cesnik and Hodges 1997] C. E. S. Cesnik and D. H. Hodges, "VABS: a new concept for composite rotor blade cross-sectional modeling", *J. Am. Helicopter Soc.* **42**:1 (1997), 27–38.

[Chang and Hodges 2009] C.-S. Chang and D. H. Hodges, "Coupled vibration characteristics of curved beams", *J. Mech. Mater. Struct.* **4**:4 (2009), 675–692.

[Chen and Ginsberg 1992] P.-T. Chen and J. H. Ginsberg, "On the relationship between veering of eigenvalue loci and parameter sensitivity of eigenfunctions", *J. Vib. Acoust.* (*ASME*) **114**:2 (1992), 141–148.

[Chidamparam and Leissa 1993] P. Chidamparam and A. W. Leissa, "Vibrations of planar curved beams, rings, and arches", *Appl. Mech. Rev.* (*ASME*) **46**:9 (1993), 467–483.

[Chidamparam and Leissa 1995] P. Chidamparam and A. W. Leissa, "Influence of centerline extensibility on the in-plane free vibrations of loaded circular arches", *J. Sound Vib.* **183**:5 (1995), 779–795.

[Fung 2004] T. C. Fung, "Improved approximate formulas for the natural frequencies of simply supported Bernoulli–Euler beams with rotational restrains at the ends", *J. Sound Vib.* **273**:1–2 (2004), 451–455.

[Hodges 1999] D. H. Hodges, "Non-linear inplane deformation and buckling of rings and high arches", *Int. J. Non-Linear Mech.* **34**:4 (1999), 723–737.

[Hodges 2003] D. H. Hodges, "Geometrically exact, intrinsic theory for dynamics of curved and twisted anisotropic beams", *AIAA J.* **41**:6 (2003), 1131–1137.

[Hodges 2006] D. H. Hodges, *Nonlinear composite beam theory*, Progress in Astronautics and Aeronautics **213**, AIAA, Reston, VA, 2006.

[Howson and Jemah 1999] W. P. Howson and A. K. Jemah, "Exact out-of-plane natural frequencies of curved Timoshenko beams", *J. Eng. Mech.* (*ASCE*) **125**:1 (1999), 19–25.

[Irie et al. 1982] T. Irie, G. Yamada, and K. Tanaka, "Natural frequencies of out-of-plane vibration of arcs", *J. Appl. Mech.* (*ASME*) **49** (1982), 910–913.

[Patil and Hodges 2006] M. J. Patil and D. H. Hodges, "Flight dynamics of highly flexible flying wings", *J. Aircraft* **43**:6 (2006), 1790–1798.

[Simitses and Hodges 2006] G. J. Simitses and D. H. Hodges, *Fundamentals of structural stabilitiy*, Elsevier, New York, 2006.

[Tarnopolskaya et al. 1996] T. Tarnopolskaya, F. R. de Hoog, N. H. Fletcher, and S. Thwaites, "Asymptotic analysis of the free in-plane vibrations of beams with arbitrarily varying curvature and cross-section", *J. Sound Vib.* **196**:5 (1996), 659–680.

[Tarnopolskaya et al. 1999] T. Tarnopolskaya, F. R. de Hoog, and N. H. Fletcher, "Low-frequency mode transition in the free in-plane vibration of curved beams", *J. Sound Vib.* **228**:1 (1999), 69–90.

[Yu et al. 2002] W. Yu, V. V. Volovoi, D. H. Hodges, and X. Hong, "Validation of the variational asymptotic beam sectional analysis", *AIAA J.* **40**:10 (2002), 2105–2112.

Received 22 Dec 2008. Revised 31 Dec 2999. Accepted 28 May 2009.

CHONG-SEOK CHANG: juliera324@hotmail.com
Advanced Rotorcraft Technology, 1330 Charleston Road, Mountain View, CA 94043, United States

DEWEY H. HODGES: dhodges@gatech.edu
Georgia Institute of Technology, Daniel Guggenheim School of Aerospace Engineering, 270 Ferst Drive, Atlanta, GA 30332-0150, United States
http://www.ae.gatech.edu/~dhodges/